
Enhancing Cosmological Simulations with Efficient and Interpretable Machine Learning in the Gabor Wavelet Basis

Anonymous Author(s)

Affiliation

Address

email

Abstract

1 Accurately simulating the large-scale structure of the universe is critical for un-
2 derstanding fundamental phenomena such as dark matter, the neutrino mass, and
3 the expansion history of the cosmos. While traditional hydrodynamic simulations
4 are essential for resolving small-scale gas dynamics, their computational demands
5 make it impractical to model the vast volumes required by next-generation cos-
6 mological surveys. To address this limitation, we present a novel approach that
7 leverages the Gabor (wavelet) transformation in combination with machine learning
8 to enhance low-resolution simulations to resemble higher resolutions. Unlike pre-
9 vious methods that relied on convolutional networks constrained by grid-specific
10 parameters, our architecture decomposes input data into a localized frequency
11 basis in a grid-shape and resolution-agnostic way, allowing for efficient feature
12 sharpening with significantly fewer learned parameters. This flexibility enables the
13 model to generalize across different resolutions and coordinate systems, including
14 non-Cartesian grids, without significant loss of accuracy. Moreover, the reduced
15 complexity of our model enhances interpretability, offering a robust tool for cos-
16 mological simulations and other fluid mechanics applications, such as weather
17 forecasting and fusion plasma modeling.

18

1 Introduction

19 The universe's large-scale structure resembles a web of gaseous clouds, is observable through galaxy
20 distribution and Lyman-alpha absorption mapping, and can be simulated using numerical methods.
21 Comparing observed and simulated maps helps researchers better understand dark matter, constrain
22 the neutrino mass, and gain insight into the history of reionization and cosmic expansion [Seljak
23 et al., 2006, Palanque-Delabrouille et al., 2015, Chabanier et al., 2019, Yèche et al., 2017, Iršič et al.,
24 2017, Armengaud et al., 2017, Walther et al., 2019].

25 Answering these fundamental cosmological questions necessitates not only precise observations
26 but also large-scale simulated model universes that match upcoming surveys. Simulations of the
27 distribution of visible matter are necessarily hydrodynamic in nature, as the emergent structures are
28 largely shaped by fluid processes. In order to accurately model the fluid behavior of intergalactic gas,
29 these simulations must resolve density features as small as a few thousand light years [Lukić et al.,
30 2015]. This minimum resolution is in conflict with the necessary volume of the next generation of
31 cosmic simulations; even on the largest supercomputers, it is impossible to run a simulation that is
32 billions of light years wide and which resolves features on the thousand light-year scale due to the
33 vast quantity of data needed to store such a simulation in computer memory. This presents a need for
34 a surrogate method to produce realistic outputs while using orders of magnitude less memory.

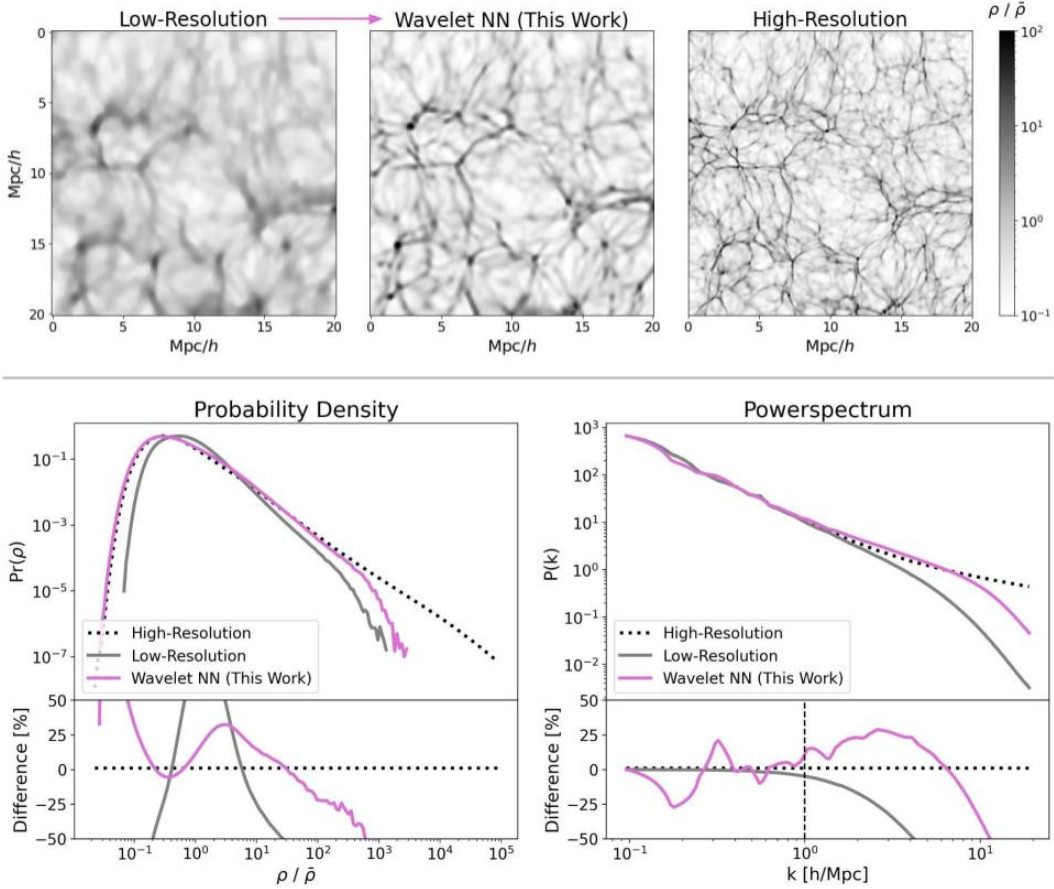


Figure 1: (TOP) Comparison of the Baryon Density fields for low and high-resolution Nyx simulations, as well as the field reconstructed by our Gabor Wavelet-based Neural Network taking the low-resolution field as input. (BOTTOM) Comparison of critical summary statistics of the three fields shown above, our wavelet model is able to introduce some of the more extreme density values and capture some of the higher-frequency elements, while keeping the resolution low.

35 1.1 Past Work in Cosmological Simulation Enhancement

36 Overcoming these constraints requires innovative deep-learning models that balance computational
 37 feasibility and accurate physical reconstructions. Machine learning has demonstrated significant
 38 promise in addressing highly non-linear problems in cosmological simulations by acting as surrogate
 39 models for complex physics [Huertas-Company and Lanusse, 2023]. Deep learning techniques have
 40 been applied to replace full simulations [He et al., 2019, Mustafa et al., 2019, Feder et al., 2020,
 41 Giusarma et al., 2023], infer gas properties from N-body simulations [Tröster et al., 2019, Thiele
 42 et al., 2020, Dai and Seljak, 2021, Bernardini et al., 2022, Harrington et al., 2022, Horowitz et al.,
 43 2022, Boonkongkird et al., 2023] and to super-resolve or sharpen coarse simulation fields [Li et al.,
 44 2021, Ni et al., 2021, Schaurecker et al., 2021, Jacobus et al., 2023].

45 Previous models used for super-resolution or sharpening coarse simulations were based on Convolu-
 46 tional Neural Net architectures (CNN) designed for standard image-to-image translators, used for
 47 applications like colorizing images. While the cosmological simulation community is excited by the
 48 results produced by these models, we recognize that they have some significant limitations, namely
 49 that they only work for the grid sizes on which they were trained, and that they employ hundreds of
 50 millions of learned parameters, making them slow to train and less interpretable. Understanding the
 51 internal behavior of the machine learning models used is of paramount importance when using them
 52 for precision cosmology. We seek to build upon the success of previous models and work towards a
 53 model which is more general and which can be better understood.

54 **1.2 Wavelets in Deep Learning and Cosmology**

55 Recently, the deep learning and cosmology communities have experimented with the application
 56 of wavelets to similar problems. In cosmology, recent work has shown that the Wavelet scattering
 57 transform can be used to extract non-Gaussian information from surveys and simulations of the
 58 large-scale structure of the universe [Cheng , Valogiannis and Dvorkin, 2022, Eickenberg et al., 2022].
 59 These works explored the merits of using wavelets to extract summary statistics to achieve better
 60 constraints on cosmological parameters, their success in extracting non-Gaussian information suggests
 61 that wavelet bases are well-suited for expressing cosmic structure. This expressivity motivates us to
 62 experiment with using these wavelet bases as pre-defined latent spaces for simulation enhancement.
 63 Wavelet Bases have been also used for efficient image super-resolution for standard image processing
 64 applications. Guo et al. [2017] use a simple 2D Haar scattering transform to decompose an input image
 65 into 4 real-valued channels before passing them through a traditional CNN, achieving impressive
 66 results for super-resolution. And Moser et al. [2023] similarly decompose an input image in the
 67 4-channel Haar basis before super-resolving it using diffusion. These models demonstrate that using
 68 wavelet bases can improve performance when combined with traditional machine learning methods.

69 **2 Model Architecture and Training**

70 We propose a new architecture to perform this cosmological simulation enhancement challenge. We
 71 use the Gabor transformation to decompose our input into a many-channel representation where
 72 features of specific wavelength ranges are represented in designated channels. As discussed further
 73 in Appendix A, the Gabor transform is complete and invertible allowing us to perform a simple
 74 point-wise learned translation in the Basis before transforming back to real space.

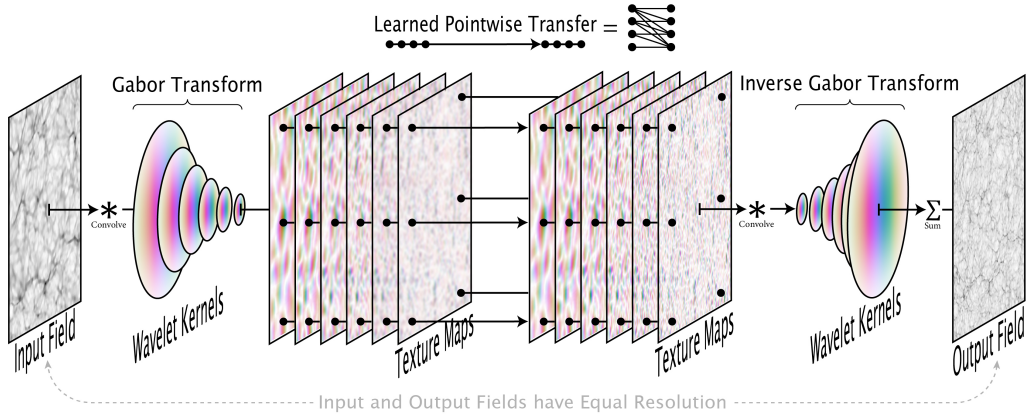


Figure 2: Diagram of our Model. An input image or volume is decomposed into localized frequency maps using the Discrete Gabor Transform. Our simple model transforms these maps with a learned point-wise function, and the Inverse Discrete Gabor Transform then recombines them into an image or volume with sharper features.

75 We train a simple multi-layer perceptron to translate between low and high-resolution simulations in
 76 this Gabor wavelet basis. Figure 2 depicts the MPL as a dark arrow connecting points in latent maps.
 77 We say this MLP is "point-wise" because at every evaluation in the inference step, only pixels at the
 78 location of the output are used. Not only does this decrease the number of parameters needed, as
 79 opposed to using a CNN, it means there are no elements of the model that depend explicitly on the
 80 resolution of the image or maps and the model can be applied generally to any resolution.
 81 We train our model on pairs of low and high-resolutions Cosmological simulations generated by the
 82 code Nyx, more information on our training data can be found in Appendix B. We train our model
 83 using L1 loss on the output maps in the Gabor basis, compared to the Gabor transform of the target
 84 image, at no point do we train on the reconstructed image which results from the inverse Gabor
 85 transform of our output maps. Further details on our model architecture can be found in Appendix C.

86 **3 Results**

87 Once training is complete, we evaluate our model on a separate volume from an unseen simulation
 88 with the same cosmological parameters, but different initial conditions. After transforming to the
 89 wavelet basis, the problem of effectively sharpening features is simpler, allowing us to use only a
 90 few thousand *learned* parameters in our network and still achieve results comparable to traditional
 91 CNNs which have with 100,000x more learned parameters. The output of the model on an unseen
 92 test sample is shown in figure 1 and compared to the low and high-resolution realizations. The
 93 improvement is not only visually apparent but is seen in the summary statistics, shown below in figure
 94 1. Our model is able to make critical adjustment in the probability density of the field, correcting
 95 the peak to match the high-resolution simulation. Our model also clearly sharpens features from the
 96 input simulation, as evidenced in the powerspectrum by the greater power at higher wavenumbers.

97 Due to the resolution-flexibility of the Gabor transform (discussed in Appendix A) and the resolution-
 98 agnostic nature of the point-wise MLP, our model can be applied to simulations of resolutions
 99 different than what it was trained on or even other grid shapes. Figure 3 below demonstrates this
 100 capability; our model has only been trained using data from the resolution shown in the central panel.
 101 We compare outputs at other resolutions and notice that the structures are faithfully preserved.

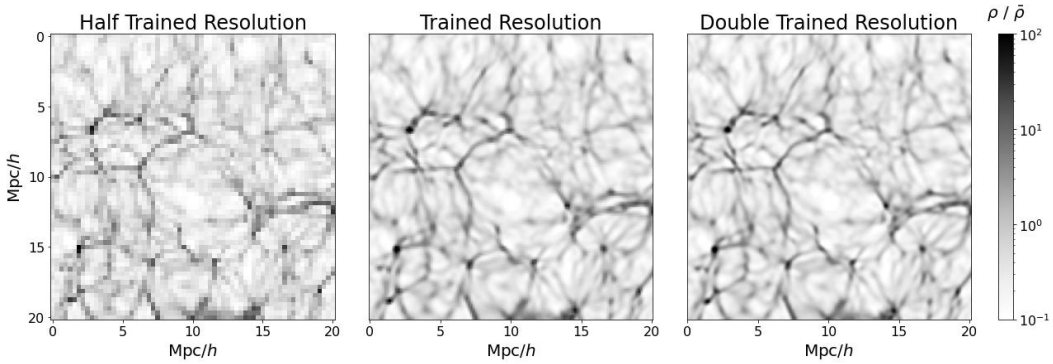


Figure 3: Comparison of Model outputs at different resolutions. The model is trained on one resolution but can be applied to different resolutions due to the nature of the wavelet transform. Here we show the model applied to cosmological simulations of the same initial conditions but with resolutions differing by factors of two.

102 **4 Limitations**

103 Although the proposed machine learning model has significantly fewer *learned* parameters, making
 104 it simpler, faster to train, and possibly more interpretable, this does not mean it is computationally
 105 faster to implement. The convolutional Gabor transform itself is very computationally expensive, due
 106 to convolutions with very large kernels (the largest kernels are 32 cells wide, much larger than the 3
 107 cell-wide kernels traditionally used in UNets and other CNNs). Additionally, the model's reliance on
 108 pre-defined Gabor filters may limit its ability to learn more complex or non-linear features compared
 109 to fully trainable architectures such as convolutional neural networks (CNNs); phase and amplitude
 110 transformations alone may not capture all necessary information.

111 **5 Conclusion**

112 By employing the Gabor basis, we find that enhancing diffuse simulations is computationally more
 113 efficient and more general, than using off-the-shelf convolutional neural networks yet still produces
 114 comparable results. This architecture allows us to use hundreds of thousands of times fewer learned
 115 parameters, a critical step towards making more interpretable machine-learning models. Our model
 116 is also naturally flexible to changes in resolution and can be applied to resolutions unseen during
 117 training. We anticipate that our architecture can be used for other problems in surrogate modeling
 118 for fluid mechanics, like efficient weather forecasting or fusion plasma modeling where a change of
 119 coordinate systems between training and inference is helpful.

120 **Broader Impact**

121 We are not aware of any negative social impacts of the work presented here. While generative
122 adversarial networks similar to the techniques used in this work can be used outside the domain of
123 cosmology for malicious cases such as deepfakes, our architecture consists of known techniques
124 already present in the machine learning community and the novelty of our work is the deployment
125 of these techniques in a practical and careful manner on cosmological modeling tasks. A potential
126 positive impact of our method is the reduction in energy consumption due to computational savings
127 avoiding the expensive full-resolution simulations.

128 **References**

- 129 A. S. Almgren, J. B. Bell, M. J. Lijewski, Z. Lukić, and E. V. Andel. Nyx: A massively parallel amr code for
130 computational cosmology. *The Astrophysical Journal*, 765(1):39, feb 2013. doi: 10.1088/0004-637x/765/1/39.
131 URL <https://doi.org/10.1088/0004-637x/765/1/39>.
- 132 E. Armengaud, N. Palanque-Delabrouille, C. Yèche, D. J. E. Marsh, and J. Baur. Constraining the mass of light
133 bosonic dark matter using SDSS Lyman- α forest. *Monthly Notices of the Royal Astronomical Society*, 471(4):
134 4606–4614, 07 2017. ISSN 0035-8711. doi: 10.1093/mnras/stx1870. URL <https://doi.org/10.1093/mnras/stx1870>.
- 136 M. Bernardini, R. Feldmann, D. Anglés-Alcázar, M. Boylan-Kolchin, J. Bullock, L. Mayer, and J. Stadel. From
137 EMBER to FIRE: predicting high resolution baryon fields from dark matter simulations with deep learning. ,
138 509(1):1323–1341, Jan. 2022. doi: 10.1093/mnras/stab3088.
- 139 C. Boonkongkird, G. Lavaux, S. Peirani, Y. Dubois, N. Porqueres, and E. Tsaprazi. Lyal-net: A high-efficiency
140 lyman- α forest simulation with a neural network, 2023.
- 141 S. Chabanier, N. Palanque-Delabrouille, C. Yèche, J.-M. Le Goff, E. Armengaud, J. Bautista, M. Blomqvist,
142 N. Busca, K. Dawson, T. Etourneau, A. Font-Ribera, Y. Lee, H. du Mas des Bourboux, M. Pieri, J. Rich,
143 G. Rossi, D. Schneider, and A. Slosar. The one-dimensional power spectrum from the SDSS DR14 Ly α
144 forests. , 2019(7):017, July 2019. doi: 10.1088/1475-7516/2019/07/017.
- 145 S. Cheng (), Y.-S. Ting (), B. Ménard, and J. Bruna. A new approach to observational cosmology using the
146 scattering transform. *Monthly Notices of the Royal Astronomical Society*, 499(4):5902–5914, 10 2020. ISSN
147 0035-8711. doi: 10.1093/mnras/staa3165. URL <https://doi.org/10.1093/mnras/staa3165>.
- 148 B. Dai and U. Seljak. Learning effective physical laws for generating cosmological hydrodynamics with
149 Lagrangian deep learning. *Proceedings of the National Academy of Science*, 118(16):e2020324118, Apr.
150 2021. doi: 10.1073/pnas.2020324118.
- 151 M. Eickenberg, E. Ally, A. M. Dizgah, P. Lemos, E. Massara, M. M. Abidi, C. Hahn, S. Hassan, B. R.-S.
152 Blancard, S. Ho, S. Mallat, J. Andén, and F. Villaescusa-Navarro. Wavelet moments for cosmological
153 parameter estimation. 2022. URL <https://api.semanticscholar.org/CorpusID:248228139>.
- 154 R. M. Feder, P. Berger, and G. Stein. Nonlinear 3D cosmic web simulation with heavy-tailed generative
155 adversarial networks. , 102(10):103504, Nov. 2020. doi: 10.1103/PhysRevD.102.103504.
- 156 E. Giusarma, M. Reyes, F. Villaescusa-Navarro, S. He, S. Ho, and C. Hahn. Learning Neutrino Effects in
157 Cosmology with Convolutional Neural Network. , 950(1):70, June 2023. doi: 10.3847/1538-4357/accd61.
- 158 T. Guo, H. S. Mousavi, T. H. Vu, and V. Monga. Deep wavelet prediction for image super-resolution. In *2017
159 IEEE Conference on Computer Vision and Pattern Recognition Workshops (CVPRW)*, pages 1100–1109, 2017.
160 doi: 10.1109/CVPRW.2017.148.
- 161 P. Harrington, M. Mustafa, M. Dornfest, B. Horowitz, and Z. Lukić. Fast, high-fidelity ly α forests with
162 convolutional neural networks. *The Astrophysical Journal*, 929(2):160, apr 2022. doi: 10.3847/1538-4357/
163 ac5faa. URL <https://doi.org/10.3847/1538-4357/ac5faa>.
- 164 S. He, Y. Li, Y. Feng, S. Ho, S. Ravanbakhsh, W. Chen, and B. Póczos. Learning to predict the cosmological
165 structure formation. *Proceedings of the National Academy of Science*, 116(28):13825–13832, July 2019. doi:
166 10.1073/pnas.1821458116.
- 167 B. Horowitz, M. Dornfest, Z. Lukić, and P. Harrington. hyphy: Deep generative conditional posterior mapping
168 of hydrodynamical physics. *The Astrophysical Journal*, 941(1):42, dec 2022. doi: 10.3847/1538-4357/ac9ea7.
169 URL <https://dx.doi.org/10.3847/1538-4357/ac9ea7>.

- 170 M. Huertas-Company and F. Lanusse. The Dawes Review 10: The impact of deep learning for the analysis of
 171 galaxy surveys. , 40:e001, Jan. 2023. doi: 10.1017/pasa.2022.55.
- 172 V. Iršič, M. Viel, M. G. Haehnelt, J. S. Bolton, S. Cristiani, G. D. Becker, V. D’Odorico, G. Cupani, T.-S. Kim,
 173 T. A. M. Berg, S. López, S. Ellison, L. Christensen, K. D. Denney, and G. Worseck. New constraints on the
 174 free-streaming of warm dark matter from intermediate and small scale lyman- α forest data. *Phys. Rev. D*,
 175 96:023522, Jul 2017. doi: 10.1103/PhysRevD.96.023522. URL <https://link.aps.org/doi/10.1103/PhysRevD.96.023522>.
- 177 C. Jacobus, P. Harrington, and Z. Lukić. Reconstructing ly fields from low-resolution hydrodynamical simulations
 178 with deep learning. *The Astrophysical Journal*, 958(1):21, nov 2023. doi: 10.3847/1538-4357/acfc5. URL
 179 <https://dx.doi.org/10.3847/1538-4357/acfc5>.
- 180 Y. Li, Y. Ni, R. A. Croft, T. Di Matteo, S. Bird, and Y. Feng. Ai-assisted superresolution cosmological simulations.
 181 *Proceedings of the National Academy of Sciences*, 118(19):e2022038118, 2021.
- 182 Z. Lukić, C. W. Stark, P. Nugent, M. White, A. A. Meiksin, and A. Almgren. The Lyman α forest in optically
 183 thin hydrodynamical simulations. , 446(4):3697–3724, Feb. 2015. doi: 10.1093/mnras/stu2377.
- 184 B. Moser, S. Frolov, F. Raue, S. Palacio, and A. Dengel. Waving goodbye to low-res: A diffusion-wavelet
 185 approach for image super-resolution, 2023. URL <https://arxiv.org/abs/2304.01994>.
- 186 M. Mustafa, D. Bard, W. Bhimji, Z. Lukić, R. Al-Rfou, and J. M. Kratochvil. CosmoGAN: creating high-fidelity
 187 weak lensing convergence maps using Generative Adversarial Networks. *Computational Astrophysics and
 188 Cosmology*, 6(1):1, May 2019. doi: 10.1186/s40668-019-0029-9.
- 189 Y. Ni, Y. Li, P. Lachance, R. A. Croft, T. Di Matteo, S. Bird, and Y. Feng. Ai-assisted superresolution
 190 cosmological simulations—ii. halo substructures, velocities, and higher order statistics. *Monthly Notices of the
 191 Royal Astronomical Society*, 507(1):1021–1033, 2021.
- 192 N. Palanque-Delabrouille, C. Yèche, J. Baur, C. Magneville, G. Rossi, J. Lesgourgues, A. Borré, E. Burtin,
 193 J.-M. LeGoff, J. Rich, M. Viel, and D. Weinberg. Neutrino masses and cosmology with lyman-alpha forest
 194 power spectrum. *Journal of Cosmology and Astroparticle Physics*, 2015(11):011–011, nov 2015. doi:
 195 10.1088/1475-7516/2015/11/011. URL <https://doi.org/10.1088/1475-7516/2015/11/011>.
- 196 D. Schaurecker, Y. Li, J. Tinker, S. Ho, and A. Refregier. Super-resolving dark matter halos using generative
 197 deep learning. *arXiv preprint arXiv:2111.06393*, 2021.
- 198 U. Seljak, A. Slosar, and P. McDonald. Cosmological parameters from combining the lyman- α forest with CMB,
 199 galaxy clustering and SN constraints. *Journal of Cosmology and Astroparticle Physics*, 2006(10):014–014,
 200 oct 2006. doi: 10.1088/1475-7516/2006/10/014. URL <https://doi.org/10.1088/1475-7516/2006/10/014>.
- 202 L. Thiele, F. Villaescusa-Navarro, D. N. Spergel, D. Nelson, and A. Pillepich. Teaching Neural Networks to
 203 Generate Fast Sunyaev-Zel’dovich Maps. , 902(2):129, Oct. 2020. doi: 10.3847/1538-4357/abb80f.
- 204 T. Tröster, C. Ferguson, J. Harnois-Déraps, and I. G. McCarthy. Painting with baryons: augmenting N-body
 205 simulations with gas using deep generative models. , 487(1):L24–L29, July 2019. doi: 10.1093/mnrasl/slz075.
- 206 G. Valogiannis and C. Dvorkin. Towards an optimal estimation of cosmological parameters with the wavelet
 207 scattering transform. *Phys. Rev. D*, 105:103534, May 2022. doi: 10.1103/PhysRevD.105.103534. URL
 208 <https://link.aps.org/doi/10.1103/PhysRevD.105.103534>.
- 209 M. Walther, J. Oñorbe, J. F. Hennawi, and Z. Lukić. New constraints on IGM thermal evolution from the ly α
 210 forest power spectrum. *The Astrophysical Journal*, 872(1):13, feb 2019. doi: 10.3847/1538-4357/aafad1.
 211 URL <https://doi.org/10.3847/1538-4357/aafad1>.
- 212 C. Yèche, N. Palanque-Delabrouille, J. Baur, and H. du Mas des Bourboux. Constraints on neutrino masses
 213 from lyman-alpha forest power spectrum with BOSS and XQ-100. *Journal of Cosmology and Astroparticle
 214 Physics*, 2017(06):047–047, jun 2017. doi: 10.1088/1475-7516/2017/06/047. URL <https://doi.org/10.1088/1475-7516/2017/06/047>.

216 Appendices

217 A The Gabor Transform

218 The Gabor Wavelet basis is an over-complete basis that can represent signals, images, volumes,
 219 etc. To transform a signal into this basis, it is convolved with a family of kernels called wavelets
 220 which extract features within certain frequency ranges and express them in a joint localization in
 221 frequency and real space. The Gabor kernels are defined as a complex-valued function composed
 222 of a Gaussian envelope modulated by a sinusoidal plane wave. The Gaussian component provides
 223 spatial localization, while the sinusoidal wave captures frequency information, making it suitable for
 224 multi-scale and multi-orientation analysis in three-dimensional signals or volumes.

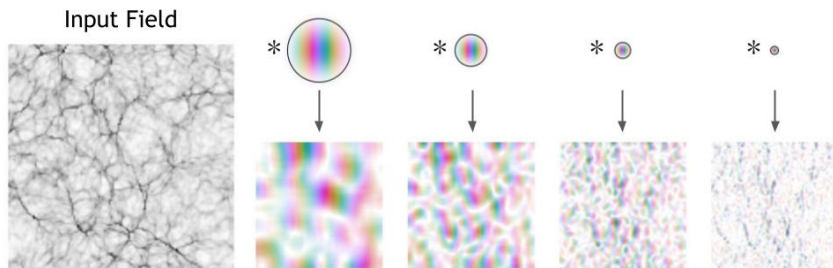


Figure 4: Decomposition of an input image into localized frequency maps using the Gabor Transform. The lower row of images show the maps produced by convolving the kernels above with the input image. Kernels and resulting maps are complex-valued, visualized with hue representing the complex phase and saturation representing the amplitude.

225 By discretizing the continuous Gabor kernel to match the spatial resolution of a given discrete image,
 226 the Gabor transform can be efficiently implemented as a series of discrete convolutions. This process
 227 applies the Gabor kernel at various scales, orientations, and frequencies, effectively decomposing
 228 the input image into multiple complex-valued channels. Each of these channels encodes localized
 229 spatial and frequency information, allowing for detailed multi-scale and multi-directional analysis
 230 of image content while preserving both magnitude and phase information in the frequency domain.
 231 By sampling these kernels to match the resolution of a discrete image, the Gabor transform can be
 232 implemented as a discrete convolution that decomposes an image into many complex-valued channels.
 233 The transform is complete (contains all information) so the channel maps can be transformed back to
 234 the original signal by convolving them again with the wavelet kernels, not unlike a Fourier transform.
 235 In 2 and 3D, the Gabor transform decomposes an image both by frequency and by orientation angle,
 236 implemented by rotating the kernel before convolution, angles are sampled in a regular manner.

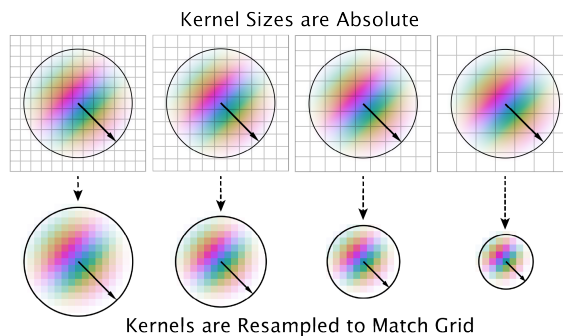


Figure 5: Gabor kernels are defined continuously and can be sampled to match the underlying grid of the discrete signal, image, or volume and implemented as a convolution. It is this feature that allows us to train on one spatial resolution and apply to others.

237 **B Training Data**

- 238 We use simulations from the cosmological hydrodynamics code Nyx [Almgren et al., 2013] as the
239 basis for our investigation. Nyx is a state-of-the-art, adaptive mesh, N-body and gas dynamics code
240 for large-scale cosmological simulations, modeling temporal evolution of the universe via a system
241 of discrete dark matter particles gravitationally coupled to an inviscid ideal fluid in a co-moving,
242 expanding box. Nyx generates volumetric inputs mapping hydrodynamic properties such as density
243 and temperature on a Eulerian grid.
- 244 To generate multiple realizations of certain cosmological environments by running Nyx simulations
245 using the same initial conditions and varying the resolution of the underlying Eulerian grid. The first
246 and last sample shown in figure 1 are generated in this way with a factor of 8 difference in the spacial
247 width of their grid cells. We train our model to translate between such pairs of simulations with the
248 same initial conditions but a factor of 8 resolution difference.

249 **C Additional model details**

250 **C.1 Model Design and Parameters**

- 251 For every orientation angle, the Gabor transform decomposes the input field into 8 complex-valued
252 channels. We pass individual points from these 8-channel maps into our model as length-16 vectors,
253 separating the real and imaginary parts. The model itself is a family of 8 Multi-Layer Perceptrons
254 (MLPs), each takes in the same length-16 vector and outputs a vector of length two, representing the
255 real and complex parts of one of the channels in the Gabor transform. These outputs are recombined
256 into a new length-16 vector and the process is repeated for every point in the input field, creating a
257 new complex-valued 8-channel feature map. This new map is then passed through the inverse Gabor
258 transform, which returns the final image. We list model details in Table 1 below.

Table 1: Hyperparameters for our network.

Hyperparameter	Value
Global batch size	1.7×10^6 point samples
Training Data size	2.7×10^9 point samples
Optimizer	Adam($\beta_1 = 0.5, \beta_2 = 0.999$)
Learning rate	5E-3
MLP Input size	16
MLP Output size	2
Number of MLPs	8
MLP Shape	Depth = 3, Width = 8

259 **C.2 Training Details**

- 260 The machine learning model itself (ie. the MLPs) is designed to produce a new Gabor decomposition,
261 not a new image. The model is therefore trained on the difference between the complex-valued,
262 8-channel map it produces and the one created by applying the Gabor transform to the target image,
263 *not the final image to the target image*. Inference is done point-wise by the MLPs, but can be
264 concatenated along the batch dimension for efficiency.
- 265 Our model is trained on the pointwise L1 difference between its predicted Gabor maps and the target
266 Gabor maps. This produces good results at the field level but reduces the computational expense of
267 training. The Gabor transform of the target images can be pre-computed and the computationally
268 expensive Inverse Gabor transform of the output need not be taken for every training step.
- 269 Our model converges (ie. the loss plateaus) after around 50 epochs of training which takes under one
270 hour to run on a single Nvidia A100 GPU. Pre-computing the Gabor transforms of all the inputs and
271 targets in the training data takes under 30 minutes on a single Nvidia A100 GPU.

272 **NeurIPS Paper Checklist**

273 **1. Claims**

274 Question: Do the main claims made in the abstract and introduction accurately reflect the
275 paper's contributions and scope?

276 Answer: [Yes]

277 Justification: We claim that our model is able to produce the desired output and show this
278 in Figure 1 with a visual and statistical comparison. We claim that our model is able to be
279 applied to other spatial resolutions one trained and present a visual demonstration of this in
280 Fig 3. We claim that our model is able to achieve these results with relatively few learned
281 parameters and present a comparison to a UNet of similar size in the appendix.

282 **2. Limitations**

283 Question: Does the paper discuss the limitations of the work performed by the authors?

284 Answer: [Yes]

285 Justification: Our submission includes a brief "Limitations" section.

286 **3. Theory Assumptions and Proofs**

287 Question: For each theoretical result, does the paper provide the full set of assumptions and
288 a complete (and correct) proof?

289 Answer: [NA]

290 Justification: Our submission does not include theoretical results.

291 **4. Experimental Result Reproducibility**

292 Question: Does the paper fully disclose all the information needed to reproduce the main ex-
293 perimental results of the paper to the extent that it affects the main claims and/or conclusions
294 of the paper (regardless of whether the code and data are provided or not)?

295 Answer: [Yes]

296 Justification: Our submission describes the architecture we have developed so that other
297 authors may apply it to their own datasets.

298 **5. Open access to data and code**

299 Question: Does the paper provide open access to the data and code, with sufficient instruc-
300 tions to faithfully reproduce the main experimental results, as described in supplemental
301 material?

302 Answer: [No]

303 Justification: Data is still proprietary, our intention is to release training data to the commu-
304 nity at a later date.

305 **6. Experimental Setting/Details**

306 Question: Does the paper specify all the training and test details (e.g., data splits, hyper-
307 parameters, how they were chosen, type of optimizer, etc.) necessary to understand the
308 results?

309 Answer: [Yes]

310 Justification: Details of the model and training setup are provided in the appendix.

311 **7. Experiment Statistical Significance**

312 Question: Does the paper report error bars suitably and correctly defined or other appropriate
313 information about the statistical significance of the experiments?

314 Answer: [No]

315 Justification: Experiments are meant to be proof-of-concept of our novel architecture,
316 predictive uncertainty is not well defined for our demonstration.

317 **8. Experiments Compute Resources**

318 Question: For each experiment, does the paper provide sufficient information on the com-
319 puter resources (type of compute workers, memory, time of execution) needed to reproduce
320 the experiments?

321 Answer: [Yes]

322 Justification: Training and implementation resources are described in the appendix.

323 **9. Code Of Ethics**

324 Question: Does the research conducted in the paper conform, in every respect, with the
325 NeurIPS Code of Ethics <https://neurips.cc/public/EthicsGuidelines>?

326 Answer: [Yes]

327 Justification: We are not aware of any violations of the NeurIPS Code of Ethics
328 Guidelines:

329 **10. Broader Impacts**

330 Question: Does the paper discuss both potential positive societal impacts and negative
331 societal impacts of the work performed?

332 Answer: [Yes]

333 Justification: We include a "Broader Impacts" section. We do not foresee any potential
334 malicious or unintended uses of our architecture.

335 **11. Safeguards**

336 Question: Does the paper describe safeguards that have been put in place for responsible
337 release of data or models that have a high risk for misuse (e.g., pretrained language models,
338 image generators, or scraped datasets)?

339 Answer: [NA]

340 Justification: The paper poses no such risks.

341 **12. Licenses for existing assets**

342 Question: Are the creators or original owners of assets (e.g., code, data, models), used in
343 the paper, properly credited and are the license and terms of use explicitly mentioned and
344 properly respected?

345 Answer: [Yes]

346 Justification: The only assets used are outputs of the Nyx hydrodynamic simulation, which
347 is cited and briefly explained in the appendix.

348 **13. New Assets**

349 Question: Are new assets introduced in the paper well documented and is the documentation
350 provided alongside the assets?

351 Answer: [NA]

352 Justification: The paper does not release new assets.

353 **14. Crowdsourcing and Research with Human Subjects**

354 Question: For crowdsourcing experiments and research with human subjects, does the paper
355 include the full text of instructions given to participants and screenshots, if applicable, as
356 well as details about compensation (if any)?

357 Answer: [NA]

358 Justification: The paper does not involve crowdsourcing nor research with human subjects.

359 **15. Institutional Review Board (IRB) Approvals or Equivalent for Research with Human
360 Subjects**

361 Question: Does the paper describe potential risks incurred by study participants, whether
362 such risks were disclosed to the subjects, and whether Institutional Review Board (IRB)
363 approvals (or an equivalent approval/review based on the requirements of your country or
364 institution) were obtained?

365 Answer: [NA]

366 Justification: The paper does not involve crowdsourcing nor research with human subjects.